Author(s): Romppanen, Sari; Häkkänen, Heikki; Kekkonen, Jere; Nissinen, Jan; Nissinen, Ilkka; Kostamovaara, Juha; Kaski, Saara

Title: Time-gated Raman and laser-induced breakdown spectroscopy in mapping of eudialyte and catapleiite

Year: 2020

Version: Accepted version (Final draft)

Please cite the original version:

Romppanen, S., Häkkänen, H., Kekkonen, J., Nissinen, J., Nissinen, I., Kostamovaara, J., & Kaski, S. (2020). Time-gated Raman and laser-induced breakdown spectroscopy in mapping of eudialyte and catapleiite. Journal of Raman Spectroscopy, 51(9), 1462-1469. https://doi.org/10.1002/jrs.5622

Time-gated Raman and Laser-induced Breakdown Spectroscopy in Mapping of Eudialyte and Catapleiite

Sari Romppanen,[1] Heikki Häkkänen,[2] Jere Kekkonen[3], Jan Nissinen[3], Ilkka Nissinen[3], Juha Kostamovaara[3] and Saara Kaski[1]

[1]University of Jyvaskyla, Department of Chemistry, P. O. Box 35 FI-40014 University of Jyvaskyla, Finland
[2]University of Jyvaskyla, Department of Biological and Environmental Science, P. O. Box 35 FI-40014 University of Jyvaskyla, Finland
[3]University of Oulu, Circuits and Systems Research Unit, P. O. Box 4500, FI-90014 University of Oulu, Finland
E-mail: sari.m.romppanen@jyu.fi

ABSTRACT

Raman analysis of rock samples containing rare earth elements (REEs) is challenging due to the strong fluorescence, which may mask the weaker Raman signal. In this research, time-gated (TG) Raman has been applied to the construction of the mineral distribution map from REE-bearing rock. With TG Raman, material is excited with a short sub-nanosecond laser pulse and the Raman signal is collected within a picosecond-scale time window prior to the formation of a strong fluorescent signal by means of single-photon avalanche diode (SPAD) array. This allows signal readout with a significantly reduced fluorescence background. TG Raman maps are used to reveal the location of valuable minerals and are compared with the elemental distribution given by laser-induced breakdown spectroscopy (LIBS). The analysis was carried out from a REE-bearing rock: nepheline syenite sample from the Norra Kärr deposit, where REEs are mainly hosted in eudialyte and catapleiite. The combination of these two complimentary laser spectroscopic methods offers valuable elemental and mineralogical information about rocks.

Keywords: time-gated Raman ; laser-induced breakdown spectroscopy (LIBS) ; mineral mapping ; rock analysis ; REE-bearing minerals

1 INTRODUCTION

The rare earth elements (REEs) are considered as critical raw materials for the European Union. This is related to the economic importance as well as the supply risk. China is

identified as the biggest global supplier of both LREEs (light rare earth elements) as well as of HREEs (heavy rare earth elements). China supplies approximately 95 % of the share of both of these.[1] As the demand for these technology metals increases, there is a need for new raw material sources. One significant REE ore resource is estimated to be the Norra Kärr Alkaline Complex located in southern Sweden. The Norra Kärr deposit is especially rich in HREE and the mineral resource is valued as 58.1 Mt with grade of 0.59 wt% total rare earth oxides (TREO). The Norra Kärr deposit is considered as a valuable source for the supply of yttrium, dysprosium and terbium.[2] Laser-induced breakdown spectroscopy (LIBS) has previously been applied at the University of Jyväskylä for the analysis of yttrium from the rocks of the Norra Kärr deposit.[3] The method is based on the atomic emission from the plasma generated from the surface of a sample by a laser pulse. The spectral lines from the atoms can be identified and thus the elemental composition of the sample point is obtained.[4] LIBS has been used in the analysis of a wide range of geological materials (*e.g.* minerals, rocks, sediments, soils and fluid inclusions)[5] and it is especially suitable for generating elemental distribution maps.[6] For example, Klus *et al*.[7] have successfully used principal component analysis (PCA) for visualizing the uranium content in sandstones. The approach used at the University of Jyväskylä based on the data processing through singular value decomposition (SVD). The original data was classified to eight groups based on the respective changes in three principal components. The assumption was that the variance in the measured spectra is caused mainly by the chemical changes between the minerals. There was a good agreement in between the yttrium distribution map to the SVD generated “mineral map” and the appearance of the sample.

In this current research, the implementation of Raman spectroscopy, which reveals the chemical bonding between the atoms through their vibrations and thus the mineralogical composition of REE-bearing rocks, is studied. The combination of these two complimentary laser spectroscopic methods would rapidly offer valuable information given by the elemental and mineralogical distributions in the sample. The fluorescence background may be one of the main limiting factors to use traditional continuous wave (CW) Raman spectroscopy for *in situ* mineral analysis because it can mask the weaker Raman signal partly or even totally. Fortunately, time responses of Raman and fluorescence photons are different and thus Raman photons scatter from a sample instantly, whereas the fluorescence photons are typically emitted within a few nanoseconds or more. As the rare earth elements are known

to be luminescence activators in minerals[8,9] causing strong fluorescence, in this research time-gated (TG) Raman is an applicable option for mapping mineral distributions.

2 MATERIAL & METHODS

Laboratory instruments:

To suppress fluorescence level of the samples, a pulsed laser can be used instead of a CW laser to illuminate the sample and then collect photons only during the laser pulse *i.e.* using a time gate as depicted in Figs. 1a and 1b.[10,11] The laser pulse and time gate have to be much shorter than the fluorescence lifetime of a sample in order to achieve proper fluorescence suppression. This means that sub-nanosecond laser pulse and time gate widths are needed to suppress the fluorescence of the minerals typically having fluorescence lifetimes of a nanosecond scale.

Traditionally, time-gated (TG) Raman has been performed by using gated ICCDs or CCDs or Kerr gates with CCDs.[10,12] These devices are still quite complex and additional gating electronics (delay unit in Fig. 1a) are needed to perform synchronized gating signals with a pulsed laser. Single-photon avalanche diodes (SPADs) can also be used to detect even a single photon and thus they are suitable for Raman photon collection. The SPAD is basic pn-junction which is reverse-biased above its breakdown *i.e*. in the Geiger mode and SPAD structures can be fabricated by using robust complementary metal oxide semiconductor (CMOS) technologies.[13] In addition, all the time-gating electronics can be integrated into the same integrated circuit with SPADs and sub-nanosecond gating can be achieved “easily” compared to CCD’s or ICCD’s.[14,15] A CMOS technology also allows to fabricate a line sensor to record the whole Raman spectrum at once.[16–18]

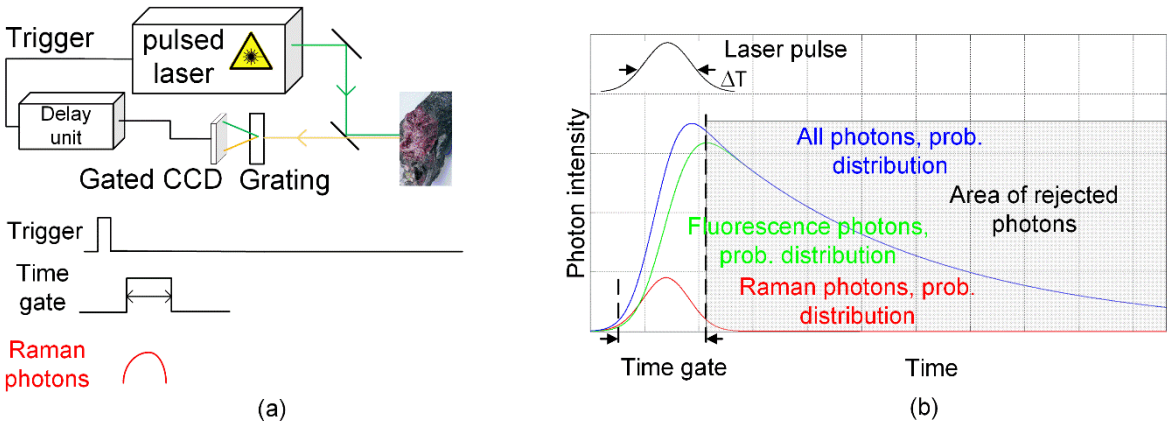

Figure 1. a) Block diagram of time-gated Raman spectrometer and b) fluorescence suppression principle.

Schematics of time-gated Raman spectrometer based on a 16 x 256 SPAD line sensor with a 256-channel time-to-digital converter (TDC) developed at the University of Oulu is shown in Fig. 2a. A sample is illuminated by using a pulsed laser having the wavelength, pulse width, energy and rate of 532 nm, 160 ps (full width half maximum (FWHM)), 1 μJ and 350 kHz, respectively. A microscope objective is used to get the spot size of approximately 150 μm on the surface of a sample. A small part of a laser pulse is delivered to the fast optical detector (DET in Fig. 2a) to give a trigger signal to the CMOS SPAD line sensor in order to bias the SPADs in Geiger mode (to detect single photons) and to give a start timing mark to the 256-channel TDC to measure the time-of-arrivals (ToA) of photons at each spectral point within the time range of approximately 600 ps. The scattered photons from a sample are split to different positions in a line sensor by means of a diffraction grating and ToA measurements are finished by the detected photons within the time bins of the TDC at each spectral point. After several thousands of laser pulses, time domain histograms can be derived at every spectral point and the Raman spectrum of a sample can be derived by post-processing these histograms by counting only the photons within the width of the laser pulse. In other words, time-gating is performed in the post-processing phase as depicted in Fig. 2a in red colour. The detailed operation of the time-gated 16 x 256 CMOS SPAD line sensor is presented elsewhere.[19] The time domain operation at a single spectral point during the Raman scanning of the sample is shown in Fig. 2b. The SPADs of a single spectral point are biased to detect photons by means of a trigger signal and at the same time the ToA of photons are counted to the bins of the TDC during several thousands of laser pulses resulting in a time domain histogram as shown in Fig. 2b. After a defined number of laser pulses, the sample is moved to the next scanning point and the measurements are repeated. For example, 1^{st} and n^{th} scanning points are presenting a mineral composition having a moderate fluorescence level and 2^{nd} and 3^{rd} scanning points have high fluorescence level resulting in time domain photon distributions and histograms as shown in Fig. 2b. In both cases the Raman spectra of the scanning points can be derived by post-processing these histograms and most of the fluorescence photons can be rejected. In addition, the dark noise was subtracted from all the measurements and the correction of the nonidealities of the line sensor was carried out with MATLAB R2016a software (The MathWorks, Inc.) compensating for the residual fluorescence baseline at the same time, as described earlier.[19]

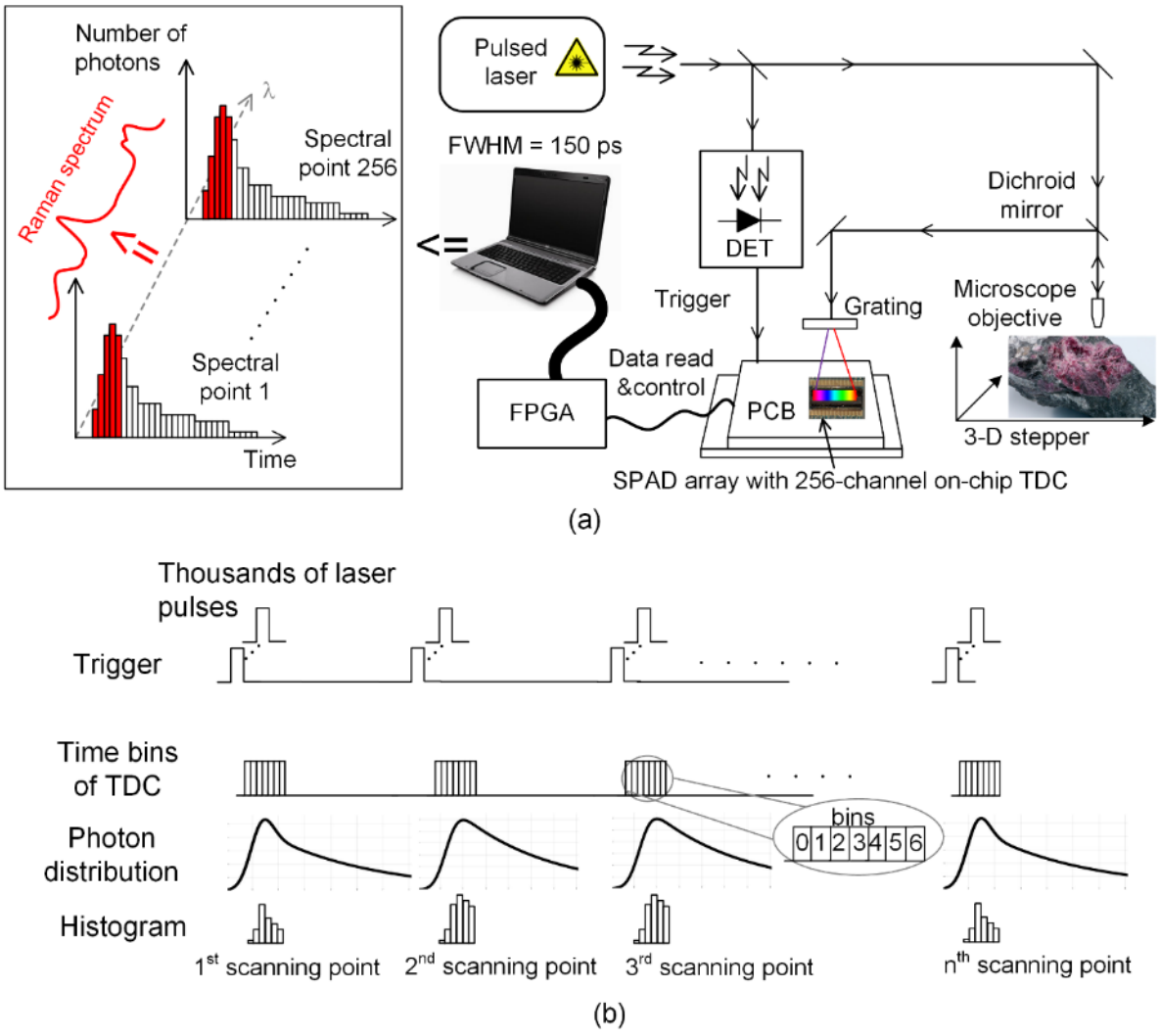

Figure 2. a) Block diagram of time-gated Raman spectrometer and b) timing diagram of the operation of a single spectral point in sample scanning.

As a reference to the time-gated Raman measurement, a continuous wave Raman was used. Setup was self-built in the backscattering geometry and had a 532 nm laser (CNI, MLL532) with a maximum power of 200 mW. An achromatic lens with a focal distance of 30 mm focused the laser beam on the rock sample. Raman scattering was collected to a CCD camera (Andor, Newton) through the imaging spectrograph (Acton SP2500i, Princeton Instruments), which had a Czerny-Turner configuration and grating of 600 grooves per mm. The spectrum was collected at each measurement point using 0.1 ms data accumulation time. As the minerals were strongly fluorescent, before each measurement sample point was photobleached at least for 0.4 seconds. The dark noise was subtracted from all the detected data during the measurement and further spectral data processing (iterative polynomial background removal) was carried out with MATLAB R2015a software.

The third measurement was carried out with laser-induced breakdown spectroscopy. The plasma was generated by focusing a 248 nm KrF excimer laser (Optex, Lambda Physik) into the surface of a sample with a 10x microscopy objective (OFR). The ablation crater diameter at the sample was approximately 30 µm and the delay and gate times for the detection of the microplasma were 70 ns and 500 ns, respectively, controlled via delay generator (model DG 535, Stanford Research System, Inc.). Emission from 389 nm – 417 nm was collected through a fused silica fiber to 150 mm Czerny-Turner type imaging spectrograph (Acton, SP-150) and equipped with an intensified charge coupled device (ICCD) with a 1024 × 256 pixel imaging area and an 18-mm intensifier (InstaSpec V, Oriel). At this range the spectral resolution was ~0.2 nm.

Analysed sample:

The sample in this research is a sawed diamond drill core half from the Norra Kärr rare earth element deposit. The main rock unit in Norra Kärr deposit is characterised as mesocratic fine-grained nepheline syenite with foliation. The major minerals include nepheline [$(Na,K)AlSiO_4$], microcline [$KAlSi_3O_8$], albite [$NaAlSi_3O_8$], aegirine [$NaFeSi_2O_6$], eudialyte [$Na_{15}Ca_6(Fe,Mn)_3Zr_3Si(Si_{25}O_{73})(O,OH,H_2O)_3(OH,Cl)_2$] and also catapleiite [$Ca/Na_2ZrSi_3O_9 \cdot 2H_2O$] occurs. Zeolites (Natrolite – Analcime [$Na_2Al_2Si_3O_{10} \cdot 2\ H_2O$ – $NaAlSi_2O_6 \cdot H_2O$] exists as secondary minerals.[20,21] This rock type is also named as grennaite after the local town Gränna.[20] In the Norra Kärr deposit occurs also the specific variation of grennaite in which ground mass has leucosomes in form of lenticles and bands of medium-grained to coarse-grained nepheline syenite. These leucosomes mainly consist on nepheline, microcline, albite, aegirine, eudialyte and catapleiite.[21] This ore type is named as PGT domain (grennaite with pegmatite). REE-levels in Norra Kärr PGT domain are high; TREO 0.62 % and ZrO_2 2.01 %.[22] The measurements were carried out from the representative sample of the PGT domain. The minerals catapleiite as well as eudialyte-group minerals, mainly eudialyte, are the focus of this research. The fluorescence lifetimes of the sample were approximated to be in ns-scale at the shortest but some points have much longer fluorescence lifetimes. The ns-scale fluorescence lifetimes were approximated by analysing time domain histograms measured by the time-gated Raman spectrometer but those longer lifetimes couldn’t be derived because of the limited range of the TDC of a sensor.

Experimental:

Macroscopically determined medium-grained area containing the precious minerals eudialyte as well as catapleiite was selected from the sample. Time-gated Raman measurement needed to be performed before the other measurements, to be sure that the fluorescence suppression was not caused by the photobleaching effect. For comparison, bigger area around the TG Raman map location was measured with CW Raman spectroscopy. After this, LIBS measurement was made from the comparable area as the TG Raman map. The measurement parameters are presented in Table 1. Although LIBS and TG Raman were carried out under the same area, due to the smaller spot size (30 µm) and step (50 µm), the LIBS area has a higher number of spectra than the TG Raman map. The photographs of the mapped areas are shown in Fig. 3. The catapleiite grains in the photograph under UV light (λ_{ex}= 248 nm) can be detected from the bright green photoluminescence, caused by uranyl ion (UO_2^{2+}) impurity in catapleiite mineral structure and it has been proven with time-gated photoluminescence measurements at the University of Jyväskylä.

Table 1. Measurement parameters.

	CW RAMAN MAP	**TG RAMAN MAP**	**LIBS MAP**
SIZE OF THE MAP	1 cm x 1 cm	2.5 mm x 1.5 mm	2.5 mm x 1.5 mm
SPECTRA IN THE MAP AREA	horizontal: 100 vertical: 100	horizontal: 11 vertical: 7	horizontal: 51 vertical: 31
TOTAL SPECTRA	10 000	77	1581
STEP	100 µm	250 µm	50 µm
SPOT SIZE	25 µm	150 µm	30 µm

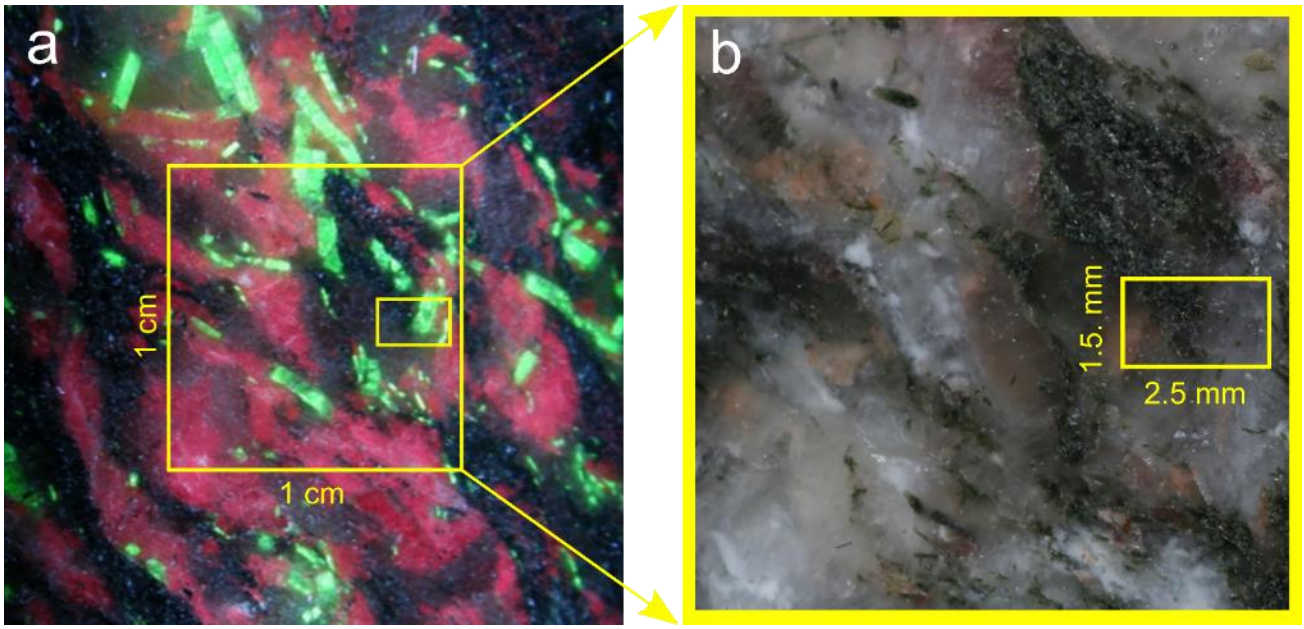

Figure 3. Measurement areas on the sample are illustrated as yellow boxes. The bigger 1 cm x 1 cm area was measured with CW Raman and the smaller 2.5 mm x 1.5 mm area with TG Raman and LIBS (a). Catapleiite grains can be recognized from intense green fluorescence when the sample surface is illuminated with 248 nm laser light. On the picture on the right (b), the CW Raman map area is presented on a bigger scale under white light to show the macroscopic mineral distribution.

3 RESULTS & DISCUSSION

Observed minerals from the Norra Kärr sample are different silicate minerals, in general. For example, spectra of chain silicate aegirine, which more precisely belongs to pyroxene group, were recognized. The basic structure of pyroxene group consists on silicon–oxygen tetrahedra joined from two corners and thus forms an infinite chain.[23] Most of the minerals belong to framework silicate group, also known as tectosilicates. These include natrolite, analcime, nepheline and microcline. Microcline is a member of the alkali feldspar series [($Na(AlSi_3O_8)$]–[$K(AlSi_3O_8)$] and albite represents the sodium endmember of a plagioclase feldspar series [$Na(AlSi_3O_8)$]–[$Ca(Al_2Si_2O_8)$].[23] For example, TO_4 ($T=Si^{4+}$, Al^{3+}) ring structure of framework silicates affects the wavenumbers of symmetric stretching mode of bridging oxygen, v_s (T-O-T), bands in the Raman spectra. In the Raman spectrum, the strongest peak of framework silicates is located below 600 cm^{-1}.[24] It has been presented that the alkali feldspars can easily be separated from the plagioclase feldspars due to the position of this peak.[25]

The representative spectra of the precious minerals of this research, eudialyte and catapleiite, are presented in Fig. 4. Eudialyte and catapleiite belong to cyclosilicates. Eudialyte contains three- and nine-fold silicon–oxygen tetrahedra rings (Si_3O_9 and Si_9O_{27}).[23,26] Meanwhile, catapleiite has only three-fold silicon–oxygen tetrahedra rings.[26] In catapleiite the most intense peaks in the region ~900–1150 cm^{-1}, are related to $(MO_n)^{x-}$ modes (M is presenting metal cation).[27] On the other hand, in eudialyte there was less characteristic peaks when compared with the other mineral spectra. Also, the Raman intensity level of the eudialyte was about a magnitude lower than in other minerals. In order to efficiently map the location of these minerals in the sample two descriptive peaks were chosen to characterize catapleiite and eudialyte mineral areas, represented as numbers 1–4 in Fig. 4. Selection was based on the least spectral interference from the other minerals and it was assumed that the use of two peaks would decrease the possible polarization effect caused by the crystal orientation. The peak 1 for the catapleiite ~630 cm^{-1} was recognized as ring stretch mode[27] and the peak 2 ~1000 cm^{-1} as $\nu(MO_2)$ mode[27]. For eudialyte, the peak 3 was ~690 cm^{-1} and the peak 4 ~1070 cm^{-1}. The latter one is typical for eudialyte group minerals and corresponds to the Si–O stretching vibrations.[28] In general, the literature describing the Raman spectra bands of eudialyte is scarce and for example, in the research of Rudolph & Peuker[29], eudialyte had been mainly recognized from the distinct REE fluorescence bands for Raman shifts larger than 3000 cm^{-1}.

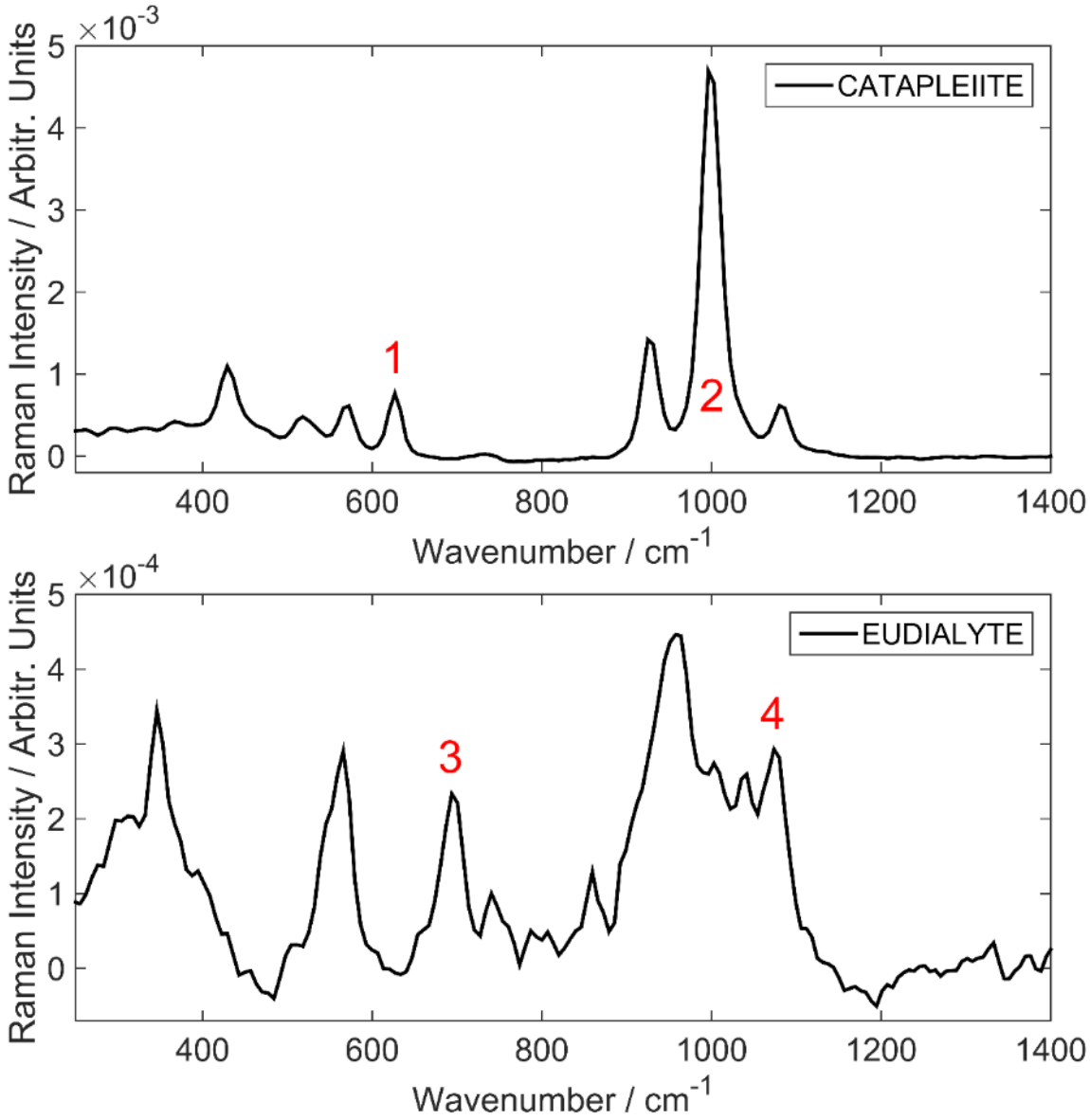

Figure 4. TG Raman spectra for catapleiite (upper) and eudialyte (lower). The intensities of the marked peaks (1–4) were used to characterize the appearance of these minerals.

To construct a map for the identification of the mineralogical areas of eudialyte and catapleiite, the spectra were first normalized to the total intensity of the spectrum and then the sum of intensities of the chosen peaks was used. The results are presented in Fig. 5 and they were compared with the LIBS data obtained from the same area. A classification map based on the multivariate analysis SVD was generated (Fig. 6a). Also Yttrium content in this area was visualized using the atomic line 410.2 nm[30] (Fig. 6b). The details of the classification procedure are presented elsewhere[3], but briefly, based on the similarities in

the LIBS spectra of different minerals, the data is divided into coloured regions in the SVD map. According to the atomic emission lines, grey areas most likely represent eudialyte, green areas catapleiite and the other colours point out other minerals, which are not in the focus of this research. Examples of LIBS spectra for eudialyte and catapleiite are presented in Fig. S1 (Supporting Information). It can be noted, that the luminescent green catapleiite grains in UV photo (Fig. 3a) correspond to the green coloured areas in the SVD map (Fig. 6a).

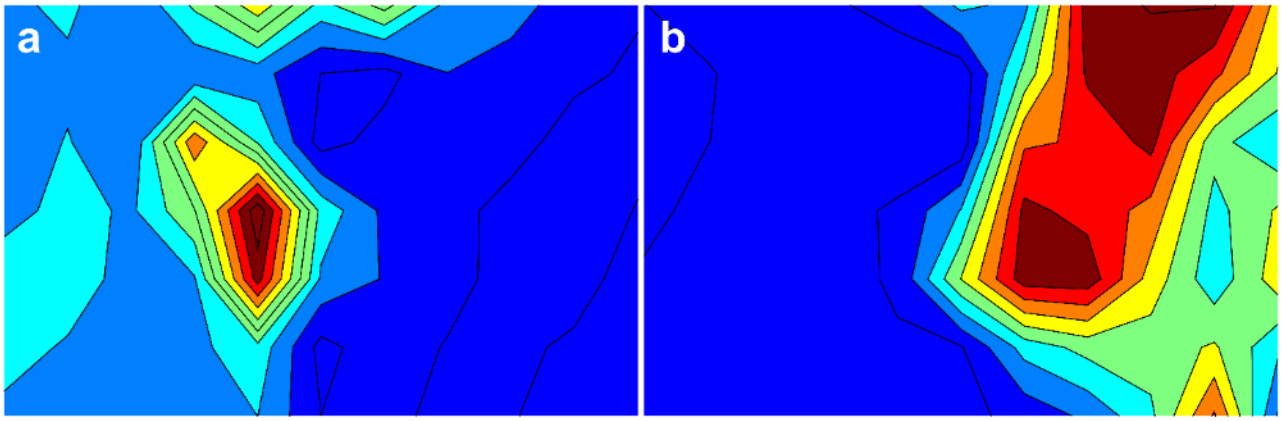

Figure 5. Mineralogical areas of eudialyte (a) and catapleiite (b) in the TG Raman maps.

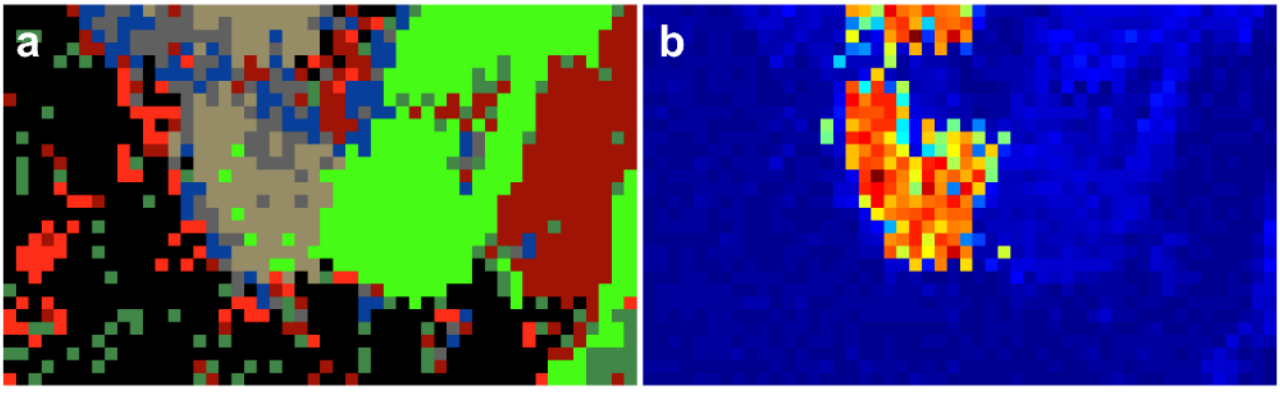

Figure 6. Maps constructed from the analyzed LIBS data. On the left (a), the map based on the separation of the spectra with singular value decomposition (SVD). In this map, grey areas are representing eudialyte and green catapleiite. On the right (b) yttrium distribution is illustrated as the intensity of the atomic emission line at 410.2 nm.

When eudialyte and catapleiite maps from TG Raman measurement (Fig. 5) are compared with the respective LIBS result of yttrium distribution (Fig. 6a), it can be noted, that the highest yttrium content is truly located in the eudialyte. We have observed weak peaks of yttrium emission in the LIBS spectrum in areas, which were confirmed by TG Raman to be catapleiite, as assumed previously.[3] Grey and green areas in the SVD classification map (Fig. 6a) show a good match to the eudialyte and catapleiite regions in the TG Raman map (Fig. 5). The differences in the shapes of mineral grains in maps are caused by the larger number of measurement points and smaller spot size with LIBS (see Table 1). At the upper edge of the eudialyte TG Raman map (Fig. 5a), there seems to be also some eudialyte, where in the LIBS map neither yttrium (Fig. 6b) nor the grey area representing eudialyte (Fig. 6a) is observed. This was due to the larger spot size of the TG Raman laser than the LIBS laser (Table 1). It can be assumed, that on the edge of the eudialyte TG Raman map partly observes eudialyte mineral outside of the LIBS region. This can be verified from the CW Raman map over the bigger area, which is represented in Fig. S2 (Supporting Information). First, maps on the top (Fig. S2a for eudialyte and Fig. S2b for catapleiite) are based on the raw CW Raman data. Despite the photobleaching, still heavy influence of fluorescence background can be detected, which influences the quality of the map and further to the mineralogical identification, especially for the eudialyte. The fluorescence can be removed mathematically from the data, which offers the clear maps of mineral distribution (Figs. S2c and S2d). When two eudialyte Raman maps (Figs. 5a and S2c) are observed more closely, light blue areas can be detected. These were found to be related mostly to nepheline mineral regions. Despite the careful selection of the eudialyte mapping peaks, some Raman peaks in nepheline spectra are a little bit overlapping. On the other hand, in the catapleiite map, especially in the TG Raman map (Fig. 5b) there are regions showing other colours than intensive red indicating high content and dark blue indicating no content. In this case, most likely small grains of catapleiite have actually been under the TG Raman laser spot in addition to the main mineral. This explanation is also supported by the coherence in the features of the catapleiite CW Raman map (Fig. S2d) and luminescence of the uranyl ion (Fig. 3a).

In principle, by combining LIBS and Raman data, the elemental information could be used to interpret the mineralogical data and vice versa, whether there was a mixture of two or more minerals in the sample location. For example, the difference in the chemical composition obtained with LIBS easily reveals nepheline and eudialyte or if the information

of the other minerals is required, Raman spectra would readily separate the different feldspars. However, in this research the potential could not be fully exploited, as the measurements were carried out separately at the University of Jyväskylä and the University of Oulu and the data points were not exactly matched.

It can be noted that although very good mapping results were obtained from the strongly fluorescent sample with CW Raman (Fig. S2, supporting information), both the photobleaching and mathematical data handling are time-consuming processes. The other thing is, that if the sample contains several minerals, which are either fluorescent or have low Raman intensity, the selection of the experimental settings turns out to be difficult with CW Raman. When exposure time needs to be chosen short in order to avoid detector saturation in the more fluorescent mineral regions, then significantly less or even not applicable signal is obtained from the non-fluorescent regions.

5 CONCLUSIONS

Time-gated (TG) Raman has been efficiently used to map mineral distributions from strongly fluorescent REE-bearing nepheline syenite. Measurement was carried out with the state-of-art time-gated Raman technology based on a CMOS fabricated single-photon avalanche diode (SPAD) line sensor with integrated time-resolving electronics. Laser-induced breakdown spectroscopy (LIBS) map revealed the locations of valuable metals (here yttrium) and offered information about the texture of the rock via robust spectral classification based on multivariate analysis (singular value decomposition, SVD). The information on the elemental distribution within the precious minerals is crucial in both ore processing and ore valuating and can also reveal the existence of some unwanted minerals for the enrichment procedure. As this research demonstrates, the combination of the information obtained from both laser spectroscopic methods could be especially useful for the mining industry, *e.g.* geologists, mining engineers or the mill operators. In general, Raman and LIBS can be built to the same setup[31], also in order to measure spectra from long distances, which has been demonstrated *e.g*. by Sharma et al.[32,33] Especially promising is that recently at the University of Oulu SPAD array detector has been successfully used to measure a Raman signal from a distance of 5 metres.[34] TG Raman measurements are not disturbed by the ambient light and the technique has potential for on-site circumstances since the setup developed at the University of Oulu is miniaturized and could be mass-produced. In the

future, combined TG Raman and LIBS may become a useful tool for fast analysis of the rare earth element bearing rocks.

ACKNOWLEDGEMENTS

The work has been funded by the Academy of Finland (decision number 281955 for SR and SK, 282240 for HH, 292609 for JKo and 282405 for JKe, IN, JN and JKo. SR would also like to thank the Finnish Society of Sciences and Letters as well as Società Italiana di Mineralogia e Petrologia for the travel grants, which gave opportunity to present the related results in GeoRaman 2018 conference. The analysed sample was provided by Tasman Metals AB (now Leading Edge Materials).

REFERENCES

[1] European Comission, *Study on the review of the list of critical raw materials - Criticality Assessments*, European Union, Brussels, **2017**.

[2] ERECON, *Strengthening the European Rare Earths Supply-chain - Challenges and policy options*, European Comission, **2015**.

[3] S. Romppanen, H. Häkkänen, S. Kaski, *Spectrochim. Acta Part B At. Spectrosc.* **2017**; *134*, 69.

[4] D. A. Cremers, L. J. Radziemski, *Handbook of Laser-Induced Breakdown Spectroscopy*, John Wiley & Sons Ltd, Oxford, 2nd edn., **2013**.

[5] R. S. Harmon, R. E. Russo, R. R. Hark, *Spectrochim. Acta Part B At. Spectrosc.* **2013**; *87*, 11.

[6] L. Jolivet, M. Leprince, S. Moncayo, L. Sorbier, C.-P. Lienemann, V. Motto-Ros, *Spectrochim. Acta Part B At. Spectrosc.* **2019**; *151*, 41.

[7] J. Klus, P. Mikysek, D. Prochazka, P. Pořízka, P. Prochazková, J. Novotný, T. Trojek, K. Novotný, M. Slobodník, J. Kaiser, *Spectrochim. Acta Part B At. Spectrosc.* **2016**; *123*, 143.

[8] M. Gaft, R. Reisfeld, G. Panczer, *Modern luminescence spectroscopy of minerals*

and materials, Springer-Verlag, Berlin/Heidelberg, **2005**.

[9] M. Gaft, Y. Raichlin, F. Pelascini, G. Panzer, V. Motto Ros, *Spectrochim. Acta Part B At. Spectrosc.* **2019**; *151*, 12.

[10] P. Matousek, M. Towrie, C. Ma, W. M. Kwok, D. Phillips, W. T. Toner, A. W. Parker, *J. Raman Spectrosc.* **2001**; *32*, 983.

[11] R. P. Van Duyne, D. L. Jeanmaire, D. F. Shriver, *Anal. Chem.* **1974**; *46*, 213.

[12] D. V. Martyshkin, R. C. Ahuja, A. Kudriavtsev, S. B. Mirov, *Rev. Sci. Instrum.* **2004**; *75*, 630.

[13] A. Rochas, M. Gani, B. Furrer, P. A. Besse, R. S. Popovic, G. Ribordy, N. Gisin, *Rev. Sci. Instrum.* **2003**; *74*, 3263.

[14] I. Nissinen, J. Nissinen, A. Lansman, L. Hallman, A. Kilpela, J. Kostamovaara, M. Kögler, M. Aikio, J. Tenhunen, in *Solid-State Device Research Conference (ESSDERC), 2011 Proceedings of the European*, IEEE, **2011**, pp. 375–378.

[15] J. Kostamovaara, J. Tenhunen, M. Kögler, I. Nissinen, J. Nissinen, P. Keränen, *Opt. Express* **2013**; *21*, 31632.

[16] I. Nissinen, A.-K. Lansman, J. Nissinen, J. Holma, J. Kostamovaara, in *2013 Proceedings of the ESSCIRC (ESSCIRC)*, **2013**, pp. 291–294.

[17] Y. Maruyama, J. Blacksberg, E. Charbon, *IEEE J. Solid-State Circuits* **2014**; *49*, 179.

[18] A. T. Erdogan, R. Walker, N. Finlayson, N. Krstaji, G. O. S. Williams, R. K. Henderson, in *2017 Symposium on VLSI Circuits Digest of Technical Papers*, **2017**, pp. C292–C293.

[19] I. Nissinen, J. Nissinen, P. Keranen, D. Stoppa, J. Kostamovaara, *IEEE Sens. J.* **2018**; *18*, 3789.

[20] O. J. Adamson, *The Petrology of the Norra Kärr District - An Occurrence of Alkaline Rocks in Southern Sweden*, Geologiska Föreningens i Stockholm Förhandlingar, Stockholm, **1944**.

[21] A. Sjöqvist, D. Cornell, T. Andersen, M. Erambert, M. Ek, M. Leijd, A. S. L. Sjöqvist, D. H. Cornell, T. Andersen, M. Erambert, M. Ek, M. Leijd, *Minerals* **2013**; *3*, 94.

[22] M. Saxon, M. Leijd, K. Forrester, J. Berg, in *Symposium on Strategic and Critical Materials Proceedings, November 13-14, 2015, Victoria, British Columbia*, (Eds: G. J. Simandl, M. Neetz), British Columbia Ministry of Energy and Mines, **2015**, pp. 97–107.

[23] W. A. Deer, R. A. Howie, J. Zussman, *An Introduction to the Rock-Forming Minerals*, Longman Scientific & Technical, Essex, 2nd edn., **1993**.

[24] J. J. Freeman, A. Wang, K. E. Kuebler, B. L. Jolliff, L. A. Haskin, *Can. Mineral.* **2008**; *46*, 1477.

[25] T. P. Mernagh, *J. Raman Spectrosc.* **1991**; *22*, 453.

[26] E. Burzo, *Cyclosilicates*, Springer-Verlag, Berlin/Heidelberg, **2005**, vol. 27I3.

[27] W. P. Griffith, *J. Chem. Soc. A Inorganic, Phys. Theor.* **1969**; *0*, 1372.

[28] R. K. Rastsvetaeva, N. V Chukanov, V. A. Zaitsev, S. M. Aksenov, K. A. Viktorova, *Crystallogr. Reports* **2018**; *63*, 400.

[29] M. Rudolph, U. A. Peuker, *Miner. Eng.* **2014**; *66–68*, 181.

[30] J. E. Sansonetti, W. C. Martin, *J. Phys. Chem. Ref. Data* **2005**; *34*, 1559.

[31] Q. Lin, G. Niu, Q. Wang, Q. Yu, Y. Duan, *Appl. Spectrosc. Rev.* **2013**; *48*, 487.

[32] S. K. Sharma, A. K. Misra, P. G. Lucey, R. C. Wiens, S. M. Clegg, *Spectrochim. Acta Part A Mol. Biomol. Spectrosc.* **2007**; *68*, 1036.

[33] S. K. Sharma, A. K. Misra, P. G. Lucey, R. C. F. Lentz, *Spectrochim. Acta Part A Mol. Biomol. Spectrosc.* **2009**; *73*, 468.

[34] J. Kekkonen, J. Nissinen, J. Kostamovaara, I. Nissinen, *Sensors* **2018**; *18*, 3200.